

Robust FOPID Control of an After-Cooler Heat Exchanger with TES

Michele Schiavo* Manuel G. Satué** Manuel Beschi*
Antonio Visioli* Manuel R. Arahal**

* *Dipartimento di Ingegneria Meccanica e Industriale, University of
Brescia, Italy (e-mail: {michele.schiavo, manuel.beschi,
antonio.visioli}@unibs.it)*

** *Systems Engineering and Automation Department, University of
Seville, 41092 Seville, Spain (e-mail: {mgarrido16, arahal}@us.es)*

Abstract: In this paper the temperature control of an after-cooler heat exchanger (AHX) with Thermal Energy Storage (TES) is considered. The AHX can be modelled as a nonlinear system whose gain strongly depends on the operating point. This can cause the reduction of the phase margin which translates into the risk of excessive temperature overshoots. The generalized isodamping approach has been applied to design a fractional-order robust PID controller that guarantees the invariance of the phase margin despite the gain variations. Simulation results performed on a realistic model of the system demonstrate the effectiveness of the proposed design approach.

Keywords: Fractional-order PID control, Robust control, Energy systems, Process control

1. INTRODUCTION

After-cooler Heat Exchangers (AHX) are devices designed to cool the source fluid after it exits the last compression stage of a compressor. This is a requisite for many industrial applications using, for instance, compressed air. The AHX uses a secondary fluid (working fluid or coolant) that takes the excess heat from the source one. In this way, at the exit of the AHX, the source fluid is cooled and the working fluid is heated. Many configurations are possible for AHX, depending on the particular fluids, operating conditions, available space, and so on. Regardless of this, there are some control challenges arising from AHX implementation. In this paper, the control problem considered is the regulation of the output temperature of the source fluid, which can be achieved by acting upon the coolant mass flow. The mass flows and inlet temperatures are considered time-varying, non-manipulable variables. This regulation problem must tackle several challenges, a summary of which is provided in the following:

- Flow-dependent phenomena. The residence time varies inversely with flow. Since both (source and coolant) mass flows can vary with time, there are non-constant delays. Also, the equivalent first-order lag changes with flow rate. Finally, the steady-state response of temperature also varies with flow rates.
- Disturbances. The input temperatures of both fluids are subject to variations due to interactions with other processes, in this case the Thermal Energy Storage (TES).
- Nonlinearities. Apart from the typical nonlinear behavior of valves, pumps, etc., heat transfer might be affected by coefficients depending on both fluid temperature and mass flow.

- Spatially distributed dynamics. The AHX is provided with temperature sensors at each end; however, the dynamics take place over some space. Lumped models approximate the behavior with some accuracy that might affect the control performance.
- Identification. Some parameters (such as transfer coefficients) are difficult to measure and, therefore, an identification procedure must be used to obtain models for control design. The identified models might degrade over time as the real AHX is subject to wear and tear, especially in the form of fouling on surfaces.

The literature is rich in control strategies for heat exchangers in general. A short review follows, focusing on the aspects that play a significant role in this study. First, and regarding modeling, several linear and nonlinear models (Alsop and Edgar, 1989) have been proposed for control purposes. Linear models are simple but can exclude some relevant aspects of the dynamics, such as resonances (Álvarez et al., 2007). More complex models based on first principles equations are less tractable for control design and require experimental work to determine the value of some coefficients (Salimpour, 2009). This hints at the use of general-purpose models (such as ARMAX) with identified coefficients (Gupta et al., 2018; Sanz Bermejo et al., 2023). In between these approaches lies semi-physical or gray-box modelling, where a priori knowledge and adjustable empirical models are combined (Casteleiro-Roca et al., 2019). Second, regarding control strategies, many different proposals have been made (Pekar, 2020), being Proportional-Integral-Derivative (PID) control the most common technique in use. Tuning of the PID can use the Ziegler-Nichols method and related approaches such as the Cohen-Coon and the Chien-Hrones-Reswick methods. Simple tuning rules have been proposed for industrial

practice (Skogestad, 2001; Sanchis and Peñarrocha-Alós, 2022). Computationally expensive optimization techniques have been proposed for the task as in (Porter and Jones, 1992) and (Trafczynski et al., 2016), where simulations are used to study the influence of fouling under PID control. Understanding the particular needs for the specific application of the AHX is key to successful tuning. For instance, the dynamic characteristics of the disturbances and the range of values of the delays can be instrumental (Oravec et al., 2018). Moreover, flow-dependent phenomena and nonlinearities can strongly degrade the control performance achievable with PID control. To deal with these issues, the use of PID-based control schemes along with feedback linearization (Alsop and Edgar, 1989) has been proposed. The main disadvantage of these approaches is that, when the operating point changes, a re-tuning of the controller parameters is required to achieve satisfactory performance. Another approach is represented by robust control strategies. The rationale is to cope with system uncertainties by designing a controller that is expected to keep the required performance within a specified uncertainty domain without the need for retuning. In (Oravec et al., 2018) a robust model predictive control strategy has been proposed, and the simulation results obtained have shown that this represents a promising strategy. In (Vasičkaninová et al., 2018) robust H_∞ and H_2 controllers have been proposed and successfully applied in a laboratory environment. However, both of these approaches come at the cost of a more complicated controller design, a higher computational load, and a more complex implementation with respect to PID-based solutions.

In this paper, we propose an alternative approach to robust control of an AHX that aims to maintain the advantages of a simple PID controller. In particular, the use of a generalized isodamping technique (Beschi et al., 2017) in combination with the tuning flexibility provided by fractional-order PID (FOPID) controllers is exploited to obtain the phase margin invariance with respect to changes in the AHX operating point. The effectiveness of this approach has already been proven in various applications, such as controlling the temperature of a solar furnace (Beschi et al., 2016) and providing an adequate level of depth of hypnosis in closed-loop control of general anesthesia (Paolino et al., 2023).

The paper is organized as follows: the case study considered in this work is presented in Section 2. In particular, the description of the considered AHX is given in Section 2.1, the control structure and the proposed tuning procedure are described in Section 2.2. The results obtained in a simulation study are shown in Section 3. Finally conclusions are given in Section 4.

2. CASE STUDY

The case study used for this work is centered on the compression stage of a plant using compressed air with Thermal Energy Storage (TES). The compressed air is cooled using water that is transferred to a vessel for later use. The TES part of the system allows for some use of the heat generated during the compression. Such heat makes for a large portion of the work provided to the compressor. By using the stored heat at a later stage in the plant, an improvement in energy efficiency is achieved

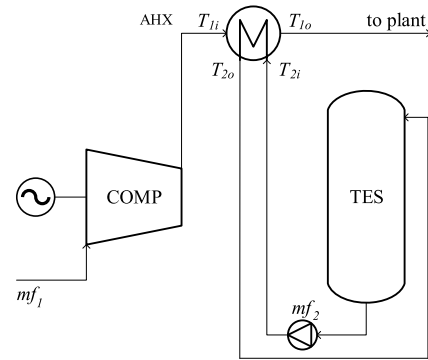


Fig. 1. Diagram of the system including the compressor (COMP), the thermal storage (TES) and the after-cooler heat exchanger (AHX).

compared with the case where heat is just dissipated into the environment.

The diagram of Fig. 1 shows the main components of the subsystem used in this case study. The mass flow of air (m_{f1} [kg/s]) is variable as needed by modern installations optimized for energy efficiency (Satué et al., 2022). A separate control loop (not shown in the diagram) is responsible for attaining the desired air mass flow following a reference from a hierarchical controller. The temperature of the air (T_{1i} [K]) is the result of the compression, where the compression rate is also a variable set by the hierarchical controller. The temperature of the water entering the AHX (T_{2i} [K]) corresponds to the bottom of the TES vessel (considering stratification); as such, it is also subject to variation as the TES is loaded or unloaded. The temperature of the water at the output of the AHX is determined by the boundary conditions and AHX effectiveness. The temperature of the air leaving the AHX (T_{1o} [K]) is the variable to be controlled. The reference value (T_{1o}^* [K]) is set by a hierarchical controller in charge of the whole plant. Finally, the manipulated variable is the mass flow of water (m_{f2} [kg/s]). This value is used as a reference by an auxiliary control loop responsible for driving the pump (not shown in the diagram).

In this paper, we focus on the effect that variations in T_{2i} , caused by TES load or unload operations, can have on the control performance of air outlet temperature. A single operating point of the compressor is considered; hence, m_{f1} and T_{1i} are treated as constants.

2.1 Description of the after-cooler

The after-cooler is of the concentric tube type. Air circulates along the inner tube and water along the outer tube in counter-current mode. Its main characteristics are presented in Table 1 along with some other relevant parameters of the subsystem under consideration. In the considered case study, the AHX is designed to operate at the nominal operating point, which is given by the set of inputs shown in Table 2. A schematic representation of the model used to describe the considered subsystem is shown in Figure 2. This model describes the relationship between the control variable m_{f2} and the controlled variable T_{1o} . The model includes a transport delay and a saturation on the control action, which depend on the maximum and minimum flow rates that the water pump in use is capable

of. The nonlinear gain between $\widetilde{m}_{f_2}(t)$, which is the control action after the transport delay and the saturation, and $\Delta T_1(t)$ is given by the relationship:

$$\Delta T_1(t) = -\frac{\dot{Q}(t)}{m_{f_1} \cdot c_{p1}} \quad (1)$$

where c_{p1} is the specific heat of air expressed in [J/(kg K)] and \dot{Q} is the thermal power expressed in [W]:

$$\dot{Q}(t) = \varepsilon(t) \cdot \dot{Q}_{max}(t). \quad (2)$$

Here, Q_{max} is the maximum theoretical value of the thermal power for the AHX expressed in [W]:

$$\dot{Q}_{max}(t) = C_{min}(t) \cdot (T_{1i} - T_{2i}(t)), \quad (3)$$

and ε is a dimensionless coefficient representing the AHX efficacy:

$$\varepsilon(t) = \frac{1 - e^{-NTU(t) \cdot (1 - C_r(t))}}{1 - C_r(t) \cdot e^{-NTU(t) \cdot (1 - C_r(t))}}, \quad (4)$$

where NTU is the number of transfer units:

$$NTU(t) = \frac{UA}{C_{min}(t)}, \quad (5)$$

with:

$$C_r(t) = \frac{C_{min}(t)}{C_{max}(t)}, \quad (6)$$

and:

$$C_{min}(t) = \min(m_{f_1} \cdot c_{p1}, \widetilde{m}_{f_2}(t) \cdot c_{p2}), \quad (7)$$

$$C_{max}(t) = \max(m_{f_1} \cdot c_{p1}, \widetilde{m}_{f_2}(t) \cdot c_{p2}). \quad (8)$$

Finally, the heat exchanger dynamics is modeled as a first-order transfer function:

$$G(s) = \frac{1}{\tau s + 1}. \quad (9)$$

It is worth noting that the AHX has a nonlinear and asymmetric behaviour. The value of the nonlinear gain is variable and depends on the operating point of the compressor (by means of m_{f_1} and T_{1i}), on the value of the control variable m_{f_2} and on T_{2i} . The effect of this nonlinear relationship can be qualitatively observed in Figure 3, which shows the steady-state relationship between m_{f_2} and T_{1i} for different values of T_{2i} . It is possible to observe that the gain of the considered subsystem changes considerably as the slope of the curves shows significant variations with respect to m_{f_2} and T_{2i} . A quantitative example is given in Table 3, where the values of the curves slopes (that is, of the linearized gains of the process) for different combinations of T_{2i} and m_{f_2} are shown. Note that these combinations correspond to those required to obtain a steady-state value of T_{1o} equal to the nominal value of 338 [K]. Hence, when T_{2i} changes m_{f_2} must be changed accordingly to obtain the same value of T_{1o} (see Figure 3). We assume that in the AHX considered it is not possible to measure T_{2i} , so that it can not be used as a scheduling variable to implement adaptive control. Hence, it is necessary to implement a controller that is robust to gain variations.

2.2 Control Structure

The control structure is shown in Figure 4, where $e(t)$ is the control error. As described in the previous section, the AHX can be modelled as a nonlinear system, whose gain strongly depends on the operating point. Thus, the control system should guarantee an acceptable performance

Table 1. Relevant parameters of the considered AHX subsystem.

Parameter	Value	Unit
Specific heat of air, c_{p1}	1018	J/(kg K)
Specific heat of water, c_{p2}	4186	J/(kg K)
Heat transfer coefficient, UA	150	W/K
Minimum pump flow rate, m_{f_2min}	0.0278	kg/s
Maximum pump flow rate, m_{f_2max}	0.5556	kg/s
AHX time constant, τ	30	s
Transport delay, L	1	s

Table 2. Values of the AHX inputs corresponding to the nominal operating point.

Input	Value	Unit
Mass flow of hot air, m_{f_1}	0.1004	kg/s
Mass flow of cooling water, m_{f_2}	0.0807	kg/s
Inlet hot air temperature, T_{1i}	453	K
Inlet cooling water temperature, T_{2i}	293	K
Outlet hot air temperature, T_{1o}	338	K

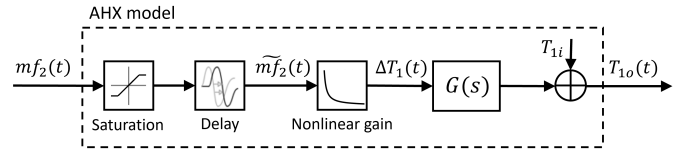


Fig. 2. Schematic representation of the nonlinear model used to describe the considered subsystem.

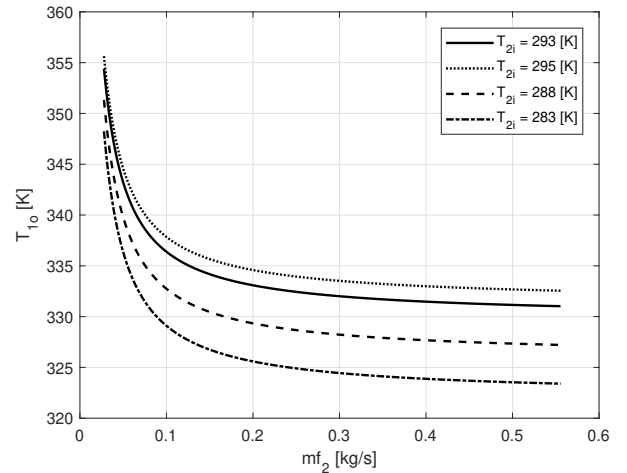


Fig. 3. Nonlinear relationship between the steady-state values of m_{f_2} and T_{1i} for different values of T_{2i} .

Table 3. Values of the linearized process gain resulting from different steady-state values of T_{2i} and m_{f_2} required to obtain $T_{1o}=338$ [K]. The second row shows the nominal operating condition.

T_{2i} [K]	m_{f_2} [kg/s]	Linearized gain [K s/kg]
295	0.0977	-70
293	0.0807	-104
288	0.0571	-218
283	0.0450	-366

independently from the gain variation. To this end, the use of the generalized isodamping technique (Beschi et al., 2017) is proposed to design a controller $C(s)$ that is able to prevent reductions of the phase margin variations because of the process gain. To apply the technique, the nominal operating conditions are considered (see Table 2) and the system is linearized around this point; thus a corresponding first-order-plus-dead-time (FOPDT) transfer function is obtained:

$$P(s) = \frac{-104}{30s + 1} e^{-s}. \quad (10)$$

The generalized isodamping approach aims to find a controller $C(s)$ that minimizes the maximum sensitivity

$$M_s := \max_{\omega} |S(j\omega)| = \max_{\omega} \left| \frac{1}{1 + L(j\omega)} \right|, \quad (11)$$

where $L(s) = C(s)P(s)$. Hence, the controller is determined by solving the following optimization problem:

$$\min_{C(s)} M_s \quad (12)$$

subject to:

- (1) $\omega_c = \bar{\omega}_c$;
- (2) $\varphi_m = \bar{\varphi}_m$;
- (3) $\left| \frac{d \arg(L(j\omega))}{d\omega} \right|_{\omega=\omega_c} = 0$;
- (4) $|S(j\omega)| < A$ for $\omega < \omega_l$;
- (5) $|T(j\omega)| = \left| \frac{L(j\omega)}{1+L(j\omega)} \right| < B$ for $\omega > \omega_h$.

Through conditions (1) and (2) the desired closed-loop system speed of response and desired overshoot can be constrained by imposing the desired gain crossover frequency and phase margin. The isodamping property is obtained through condition (3) by imposing the phase of $L(s)$ to be locally flat in the neighbourhood of the gain crossover frequency. This implies the local invariance of the phase margin with respect to variations in the gain of $P(s)$. Thanks to this property, it is possible to keep almost constant the overshoot of the closed-loop system response in the time domain. This is an important feature in AHX control as significant temperature overshoot may be dangerous as they can damage some components of the system. Conditions (4) and (5) are used to obtain a good attenuation of low frequency output/load disturbances and of high frequency noise, respectively.

By considering the control specifications for the considered AHX subsystem, the following optimization constraints have been imposed:

- $\bar{\omega}_c = 0.025$ rad/s;
- $\bar{\varphi}_m = 75^\circ$;
- $A=0.1$ and $\omega_l = 0.1\bar{\omega}_c$;
- $B=0.1$ and $\omega_h = 10\bar{\omega}_c$.

Note that a desired phase margin of 75° has been selected to obtain a maximum overshoot of 10%.

It is worth noting that when the structure of $C(s)$ is given, like in the case where a PID controller is used, the optimization problem consists of finding a set of tuning parameters that minimize M_s while satisfying all the constraints. As a first attempt, $C(s)$ has been selected as a PID controller implemented in ideal form, that is:

$$C(s) = K_p \left(1 + \frac{1}{T_i s} + \frac{T_d s}{1 + \frac{T_d}{N} s} \right), \quad (13)$$

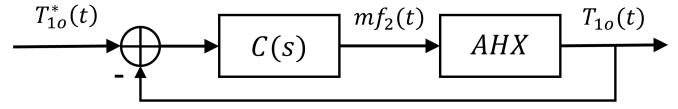


Fig. 4. Schematic representation of the control structure considered.

with $N = 10$. The optimization problem consisted of finding a set of tuning parameters K_p , T_i and T_d that solve the constrained optimization problem. To this end, a genetic algorithm implemented in MATLAB has been employed. However, it is not possible to find a feasible solution. Thus, $C(s)$ has been selected as a FOPID controller as it enables the expansion of the feasible solutions set compared to a standard PID controller, without substantially increasing the complexity of the optimization problem. Indeed, only two additional tuning parameters are added (namely, the fractional order terms of the integral action λ and of the derivative action μ) (Beschi et al., 2017). The transfer function of the FOPID controller is:

$$C(s) = K_p \left(1 + \frac{1}{T_i s^\lambda} + \frac{T_d s^\mu}{1 + \frac{T_d}{N^\mu} s^\mu} \right), \quad (14)$$

with $N = 10$. With this controller, a feasible solution can be found and the optimal parameters are $K_p = 0.0061$, $T_i = 29.1845$, $\lambda = 1.0775$, $T_d = 0.4027$ and $\mu = 1.1342$, which correspond to $M_s=1.0124$. The controller is then implemented by exploiting the CRONE approximation (Oustaloup et al., 2000) obtained with 8 pairs of zeros and poles within a frequency band of $[0.1\omega_c, 10\omega_c]$. To account for the control action saturation, the back-calculation anti-windup scheme proposed in Padula et al. (2012) has been used.

3. SIMULATION RESULTS

To evaluate the performance of the designed FOPID controller a set-point tracking simulation scenario has been considered. Initially, the closed-loop system keeps T_{1o} at its nominal value of 338 [K] and the system is at the steady-state. Then, after 10 seconds, a step set-point change is applied to T_{1o}^* . To assess the robustness of the system with respect to variations of the process gain, the same simulation scenario is applied for different values of T_{2i} . Note that, since the closed-loop system is considered, a different value of T_{2i} results in different initial values of the control action m_{f2} at the beginning of simulation (see Table 3).

As a first example, the unitary step response of the linearized system has been considered. To reproduce the effect of the T_{2i} perturbations, the linearized process gain has been changed according to the values shown in Table 3. The results obtained are shown in Figure 5. It is possible to observe that, thanks to the isodamping property, the overshoot of the responses remains constant even in presence of the considerable variability of the process gain.

Then, to assess the behavior of the controller on the nonlinear system the simulations are performed by using the model shown in Figure 2. The responses obtained for a unitary positive step change on T_{1o}^* are shown in Figure 6. It is possible to observe that the responses obtained

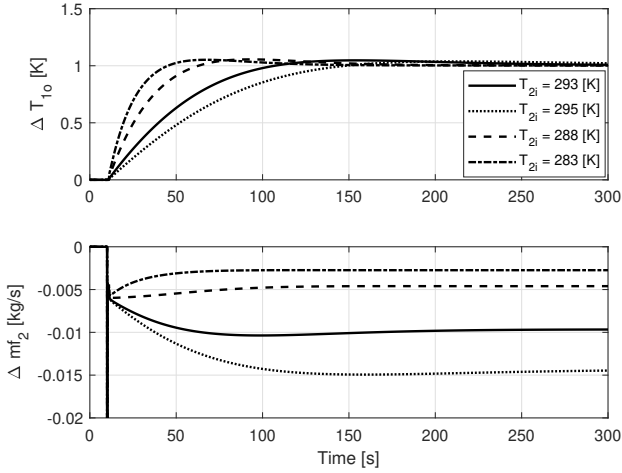


Fig. 5. Responses obtained on the linear model for a unitary step change applied on T_{1o}^* for different values of T_{2i} .

are very similar to those obtained on the linear model and the isodamping property holds true also in this case. To assess the effect on control performance caused by the asymmetric behavior of the system, the responses to a unitary negative step change on T_{1o}^* are shown in Figure 7. In this case, it is possible to observe that the asymmetric behavior causes a reduction in the closed-loop bandwidth, which is witnessed by slower responses with respect to those obtained with the positive step change on the reference signal. However, thanks to the isodamping property, the undershoot remains constant also in this case.

To further assess the behavior of the controller with respect to the effect of the system nonlinearities the simulations have been repeated by applying a positive and a negative step change on T_{1o}^* of amplitude 5. The results obtained are shown in Figures 8 and 9, respectively. In these cases the effects of the system nonlinearities are more visible on the responses obtained. As regards the positive step change, it is possible to observe an increment of the closed-loop bandwidth, which, however, is not paid at the cost of a more pronounced overshoot. Note that, for the responses obtained with $T_{2i}=283$ [K], the effect of the increased process gain is mitigated by the saturation of the control action and the bandwidth is no further incremented. Also in this case, the overshoot remains limited, thus indicating the effectiveness of the anti-windup technique employed. As regards the negative step change, in Figure 9 it is possible to observe that the responses become particularly sluggish (note that the simulation time has been increased from 300 s to 2000 s to include the end of the transient for the case with $T_{2i}=295$ [K]). This is due to the fact that, to reach the set-point value of $T_{1o}^*=333$ [K], it is required to increase the value of the control action m_{f2} , which translates into a significant reduction of the process gain (see Figure 3). However, also in this case, the isodamping condition shows the effectiveness of the method to enlarge the working range of the control system.

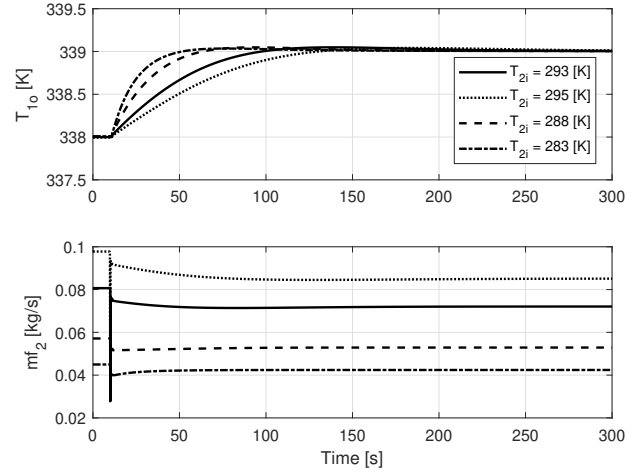


Fig. 6. Responses obtained on the nonlinear model for a positive unitary step change applied on T_{1o}^* for different values of T_{2i} .

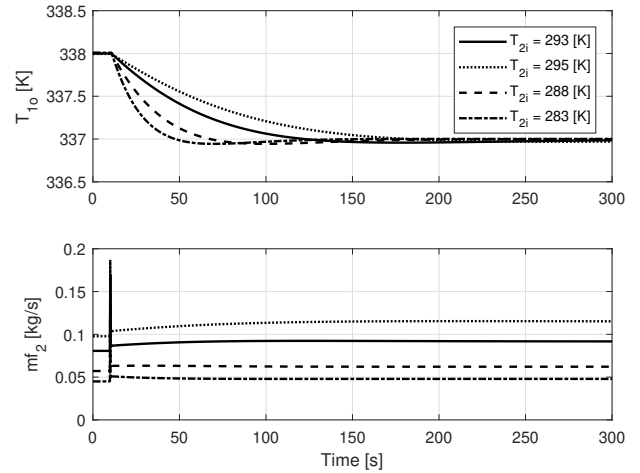


Fig. 7. Responses obtained on the nonlinear model for a negative unitary step change applied on T_{1o}^* for different values of T_{2i} .

4. CONCLUSIONS

This paper deals with the temperature control problem of an AHX with TES. The control task is particularly challenging due to the AHX's strongly nonlinear and asymmetric behavior that leads to a significant variation of the process gain. This variation is highly dependent on the AHX operating point. Such a situation is dangerous as it may lead to a reduction in the phase margin, thus exposing to the risk of excessive temperature overshoots that can potentially damage system components. To address this issue, the generalized isodamping approach has been employed to design a fractional robust PID controller. This controller, thanks to the isodamping property, ensures the invariance of the phase margin despite variations in gain. A simulation study has been performed by exploiting a realistic nonlinear model of the AHX to evaluate the controller's performance and its behavior with respect to the effects of nonlinearities. The obtained results have demonstrated the effectiveness of the proposed design approach.

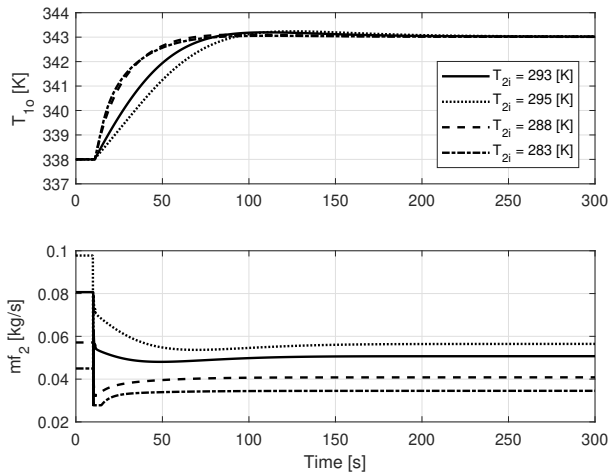


Fig. 8. Responses obtained on the nonlinear model for a positive step change of amplitude 5 applied on T_{10}^* for different values of T_{2i} .

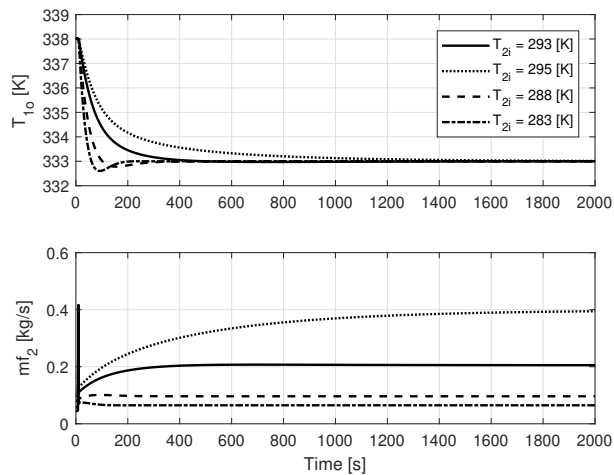



Fig. 9. Responses obtained on the nonlinear model for a negative step change of amplitude 5 applied on T_{10}^* for different values of T_{2i} .

ACKNOWLEDGEMENTS

 Funded by the European Union under GA No 101115601 (PUSH-CCC). Views and opinions expressed are however those of the author(s) only and do not necessarily reflect those of the European Union or EISMEA. Neither the European Union nor the granting authority can be held responsible for them.

REFERENCES

Alsop, A.W. and Edgar, T.F. (1989). Nonlinear heat exchanger control through the use of partially linearized control variables. *Chemical Engineering Communications*, 75(1), 155–170.

Álvarez, J., Yebra, L., and Berenguel, M. (2007). Repetitive control of tubular heat exchangers. *Journal of Process Control*, 17(9), 689–701.

Beschi, M., Padula, F., and Visioli, A. (2016). Fractional robust PID control of a solar furnace. *Control Engineering Practice*, 56, 190–199.

Beschi, M., Padula, F., and Visioli, A. (2017). The generalised isodamping approach for robust fractional PID controllers design. *International Journal of Control*, 90(6), 1157–1164.

Casteleiro-Roca, J.L., Barragán, A.J., Segura, F., Calvo-Rolle, J.L., and Andújar, J.M. (2019). Intelligent hybrid system for the prediction of the voltage-current characteristic curve of a hydrogen-based fuel cell. *Revista Iberoamericana de Automática e Informática industrial*, 16(4), 492–501.

Gupta, S., Gupta, R., and Padhee, S. (2018). Parametric system identification and robust controller design for liquid–liquid heat exchanger system. *IET Control Theory & Applications*, 12(10), 1474–1482.

Oravec, J., Bakošová, M., Trafczynski, M., Vasičkaninová, A., Mészáros, A., and Markowski, M. (2018). Robust model predictive control and PID control of shell-and-tube heat exchangers. *Energy*, 159, 1–10.

Oustaloup, A., Levron, F., Mathieu, B., and Nanot, F.M. (2000). Frequency-band complex noninteger differentiator: characterization and synthesis. *IEEE Transactions on Circuits and Systems I: Fundamental Theory and Applications*, 47(1), 25–39.

Padula, F., Visioli, A., and Pagnoni, M. (2012). On the anti-windup schemes for fractional-order PID controllers. In *Proceedings of 2012 IEEE 17th International Conference on Emerging Technologies & Factory Automation (ETFA 2012)*, 1–4.

Paolino, N., Schiavo, M., Latronico, N., Padula, F., Paltenghi, M., and Visioli, A. (2023). On the use of FOPID controllers for maintenance phase of general anesthesia. *Applied Sciences*, 13(13), 7381.

Pekar, L. (2020). *Advanced Analytic and Control Techniques for Thermal Systems with Heat Exchangers*. Academic press.

Porter, B. and Jones, A. (1992). Genetic tuning of digital PID controllers. *Electronics letters*, 9(28), 843–844.

Salimpour, M.R. (2009). Heat transfer coefficients of shell and coiled tube heat exchangers. *Experimental thermal and fluid science*, 33(2), 203–207.

Sanchis, R. and Peñarrocha-Alós, I. (2022). A new method for experimental tuning of PI controllers based on the step response. *ISA transactions*, 128, 329–342.

Sanz Bermejo, F.J., Ramírez Laboreo, E., and Sagüés Blázquez, C. (2023). Structural identifiability analysis of a heat transfer system. *Revista Iberoamericana de Automática e Informática industrial*, 20(4), 412–420.

Satué, M.G., Arahál, M.R., Acedo, L.F., and Ortega, M.G. (2022). Economic versus energetic model predictive control of a cold production plant with thermal energy storage. *Applied Thermal Engineering*, 210, 118309.

Skogestad, S. (2001). Probably the best simple PID tuning rules in the world. In *AIChE Annual Meeting, Reno, Nevada*, volume 77, 276h. Citeseer.

Trafczynski, M., Markowski, M., Alabrudzinski, S., and Urbaniec, K. (2016). The influence of fouling on the dynamic behavior of PID-controlled heat exchangers. *Applied Thermal Engineering*, 109, 727–738.

Vasičkaninová, A., Bakošová, M., Čírka, L., Kalúz, M., and Oravec, J. (2018). Robust controller design for a laboratory heat exchanger. *Applied Thermal Engineering*, 128, 1297–1309.